THE JOURNAL OF PHYSICAL CHEMISTRY C
A JOURNAL OF THE AMERICAN CHEMICAL SOCIETY

pubs.acs.org/JPCC

Article

Band-Gap Energy and Electronic *d*−*d* Transitions of $NiWO_4$ Studied under High-Pressure Conditions

Daniel Errandonea,* Fernando Rodriguez, Rosario Vilaplana, David Vie, Siddhi Garg, Bishnupriya Nayak, Nandini Garg, Jaspreet Singh, Venkatakrishnan Kanchana, and Ganapathy Vaitheeswaran*

Cite This: *J. Phys. Chem. C* 2023, 127, 15630−15640

Read Online

ACCESS | Metrics & More | Article Recommendations | Supporting Information

ABSTRACT: We report an extensive study of the optical and structural properties of $NiWO_4$ combining experiments and density functional theory calculations. We have obtained accurate information on the pressure effect on the crystal structure determining the equation of state and compressibility tensor. We have also determined the pressure dependence of the band gap finding that it decreases under compression because of the contribution of Ni 3*d* states to the top of the valence band. We report on the sub-band-gap optical spectrum of $NiWO_4$ showing that the five bands observed at 0.95, 1.48, 1.70, 2.40, and 2.70 eV correspond to crystal-field transitions within the $3d^8$ (t_{2g}^6 e_g^2) configuration of Ni^{2+}. Their assignment, which remained controversial until now, has been resolved mainly by their pressure shifts. In addition to the transition energies, their pressure derivatives are different in each band, allowing a clear band assignment. To conclude, we report resistivity and Hall-effect measurements showing that $NiWO_4$ is a *p*-type semiconductor with a resistivity that decreases as pressure increases.

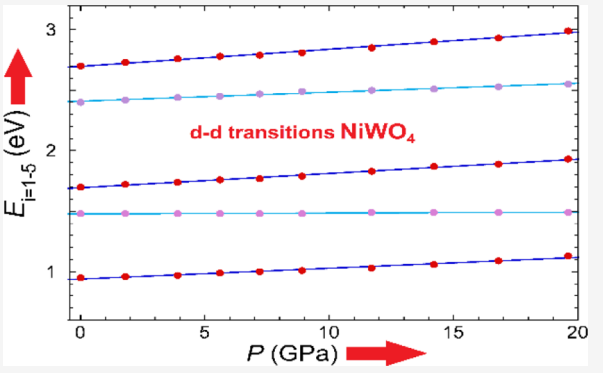

1. INTRODUCTION

Because of global warming the development of renewable energy sources and environmentally friendly energy storage is a hot topic. Photocatalytic water splitting and supercapacitors are two of the most promising technologies. Nickel tungstate ($NiWO_4$) has been studied as an efficient material for both technologies.[1,2] This and other tungstates are also extraordinary scintillator materials for high-energy physics.[3] The accurate understanding of the properties of $NiWO_4$ is fundamental for the above-mentioned technological applications. $NiWO_4$ crystallizes in a monoclinic structure described by space group $P2/c$.[4] It is isomorphic to the mineral wolframite - $(Fe,Mn)WO_4$ −[5] sharing the structure with several tungstates, including $CoWO_4$, $CdWO_4$, $MgWO_4$, $MnWO_4$, and $ZnWO_4$.[6] High-pressure studies have contributed to the understanding of the structural and electronic properties of wolframites.[7−10] High pressure (HP) can substantially modify the structural and electronic properties of materials favoring a deep understanding of them.[11] $NiWO_4$ is one of the wolframites that has been less studied under compression, there being only one article recently published.[10] In this work, a phase transition was reported around 20 GPa, which is in consistent with results previously reported for other wolframites.[6] In addition, the pressure dependence of the band-gap energy (E_{gap}) and two Ni^{2+} *d*−*d* intra-band transitions were reported. However, there are several issues regarding the electronic properties of $NiWO_4$, and their HP behavior that still needs to be clarified. For instance, the assignment of Ni^{2+} *d*−*d* transitions made by Ye et al.[10] from measurements carried out in the 1.45−3.5 eV region is at odds with the assignment made by Ejima et al.[12] and by de Oliveira et al.[13] from experiments performed in the 0.82−6.0 eV region and in the 1.3−6.5 eV region, respectively. On the other hand, for the band-gap energy, a value of 2.87 eV has been reported in the most recent work.[10] However, a large dispersion of band-gap energies can be found in the literature for $NiWO_4$. For instance, E_{gap} = 3.4 eV was reported in ref 12, E_{gap} = 3.7 eV in ref 13, E_{gap} = 2.73−2.93 in ref 14, E_{gap} = 2.1 eV in ref 15, E_{gap} = 2.2−2.6 eV in ref 16, E_{gap} = 2.77 eV in ref 17, and E_{gap} = 2.28 eV in ref 18. These results clearly show that it is timely to perform additional studies on $NiWO_4$. Photocatalytic water splitting and photocatalytic wastewater treatment require semiconductors with the band-gap energy in the visible part

Received: May 24, 2023
Revised: July 7, 2023
Published: July 26, 2023

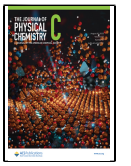

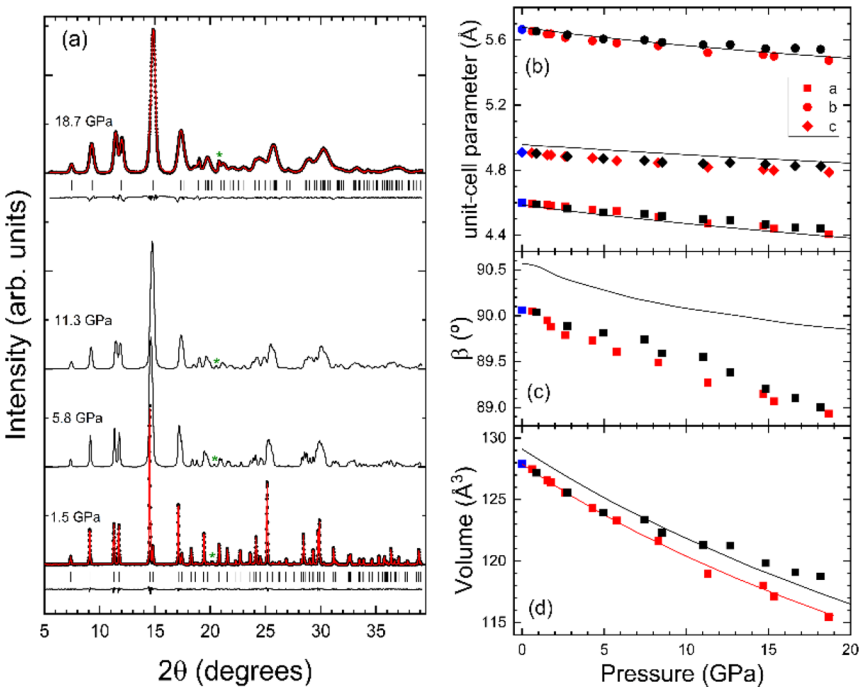

Figure 1. (a) XRD patterns measured at different pressures which are indicted in the figure. In the top and bottom traces, we show experiments (black dots), refinements (red lines), residuals (black lines), and positions of reflections (vertical ticks). The green asterisks identify the peak of Cu used to determine pressure. (b) Pressure dependence of the lattice parameters *a*, *b*, and *c*. (c) Pressure dependence of the β angle. (d) Pressure dependence of the unit-cell volume. Blue symbols are from our experiment performed outside the DAC. Red symbols are from our HP experiments, and black symbols are from ref 10. The black lines are from our DFT calculations, and the red line represents the 3rd order Birch–Murnaghan EOS determined from our experiments.

of the solar spectrum, in particular with values from 2.0 to 2.6 eV.[19] The accurate knowledge of the band-gap energy is therefore crucial for the use of $NiWO_4$ for these applications.

In this work, we report a HP study of $NiWO_4$ up to 20 GPa. Our study includes HP synchrotron X-ray diffraction (XRD) experiments and optical-absorption experiments in the 0.82–3.6 eV region up to 20 GPa, resistivity and Hall-effect measurements up to 10 GPa, and density-functional theory (DFT) calculations up to 20 GPa. The combination of all the methods allows us to accurately determine the electronic properties of $NiWO_4$ and the effect of pressure on them up to 20 GPa. We show that changes in the fundamental band gap and Ni^{2+} internal d–d absorption bands are intimately related to structural changes. The assignment of Ni^{2+} d–d transitions is discussed, clarifying previous discrepancies in the literature.

2. METHODS

Polycrystalline $NiWO_4$ has been synthesized from a stoichiometric mixture of nickel(II) acetate hexahydrate $Ni(CH_3CO_2)_2 \cdot 6H_2O$ (Fluka, 98%) and ammonium metatungstate $(NH_4)W_{12}O_{39}$ (Aldrich, 99.0%). The starting Ni- or W-containing solutions were prepared by dissolving their respective salts in distilled water. Then they were combined to obtain Ni-W source solutions having a total cationic concentration of 0.3 M and a total volume of 21.7 mL. The masses of the different reagents were adjusted to obtain 1 g of the final product. Droplets of the solution were flash-frozen by projection onto liquid nitrogen and then freeze-dried at a pressure of 1–10 Pa in a Telstar Cryodos freeze-dryer. In this way, a dried solid precursor was obtained as amorphous loose powder. Thermal evolution of the precursor was monitored by means of thermogravimetric experiments under an oxygen atmosphere (heating rate 10 K min^{-1}, flow rate 60 cm^3 min^{-1}), carried out using a TA Instruments TG550 thermogravimetric analyzer. The final $NiWO_4$ polycrystalline product was obtained by decomposing the precursor in an oven at 800 °C for 1 h. The purity and crystal structure of the synthesized $NiWO_4$ was confirmed by powder XRD using a Bruker D8 Advance A25 system and Cu K_α radiation. We have not detected any impurity in the XRD experiments. The unit-cell parameters at ambient conditions are a = 4.599(3) Å, b = 5.664(5) Å, c = 4.910(5) Å, β = 90.06(7)°. These values agree with those determined from single-crystal neutron diffraction experiments.[20]

HP synchrotron powder XRD measurements were carried out at the Extreme Conditions XRD beamline (BL-11)[21] in the Indus-2 synchrotron using monochromatic X-rays (λ = 0.731 Å) and a diamond-anvil cell (DAC). We used diamond anvils with a culet size of 400 μm and a tungsten gasket with a thickness of 50 μm with a centered hole of 200 μm in diameter. The pressure medium was a 16:3:1 methanol–ethanol–water mixture (MEW)[22] and copper was used as a pressure marker.[23] Diffraction images were collected in a MAR345 imaging-plate detector. Their integration into intensity vs 2θ patterns was made using Dioptas.[24] The XRD results patterns were analyzed using the graphical interface of GSAS.[25]

Optical-absorption measurements were carried out in a DAC using a 3-μm-thin platelet of $NiWO_4$ obtained by compacting $NiWO_4$ powder between diamond anvils. The characteristics of the DAC were the same as in XRD measurements. The pressure medium was also the same, and the gasket had similar dimensions but was made of Inconel. Pressure was determined using the ruby fluorescence method.[26] Measurements in the

https://doi.org/10.1021/acs.jpcc.3c03512
J. Phys. Chem. C 2023, 127, 15630–15640

0.82−3.6 eV range were performed in an optical setup, which consisted of a tungsten lamp, fluorite lenses, reflecting optics objectives, and several Ocean Optics spectrometers.[27]

Hall-effect and resistivity measurements were performed with a hydraulic press and steel-belted Bridgman tungsten-carbide anvils[28] using annealed pyrophyllite gaskets and boron nitride as pressure medium and to electrically isolate the sample from the anvils. Samples were compact pellets made from the $NiWO_4$ powder. Electrical contacts were made with silver wires and soldered with indium to the sample in a Van der Pauw configuration. The pressure was calibrated against the transition pressures of Bi, Yb, CdTe, and InSe.[29]

The *Vienna Ab-initio Simulation Package* (VASP) code,[30,31] which is based on plane waves, was used to study the electronic and structural characteristics of $NiWO_4$ at HP. The exchange correlation functionals were computed using the Perdew−Burke−Ernzerhof (PBE) potentials within the Generalized-Gradient Approximation (GGA),[32] and Projector augmented wave (PAW)[33] potentials were used to approximate the ion-electron interactions. In calculations we treated Ni $3d^8$ $4s^2$, W $6s^2$ $5d^4$, and O $2s^2$ $2p^4$ explicitly as valence electrons and the rest of electrons as core electrons. To ensure accuracy and high precision in the calculations, we used a plane-wave energy cutoff of 600 eV. The energy convergence criteria have been chosen to be 10^{-6} eV. The geometry optimization calculations have been performed at 0 K by doubling the unit-cell along the *a*-axis to consider magnetic configurations and using a 4 × 6 × 8 k-mesh in accordance with the Monkhorst−Pack method.[34] According to the various investigations of transition metal compounds, the GGA frequently produces the wrong findings in case of highly correlated systems. In this case, the inclusion of Hubbard parameter (U) has been found to have some impact on transition metal compounds.[35] The significant correlation effects of nickel *d* states were treated by using a Hubbard (U) parameter (GGA + U) of 6.5 eV.[36] Because $NiWO_4$ presents a magnetic moment, we considered non-magnetic, ferromagnetic, and different antiferromagnetic configurations.[37] We found that the configuration with the lowest energy is an antiferromagnetic order with a magnetic unit cell (2*a*, *b*, *c*) which doubles the crystallographic one along the *a*-axis. The spins at nickel atoms are arranged collinearly making a linear chain running nearly along the crystallographic $[0,\bar{1},1]$ direction, but are antiparallel to the spins in adjacent chains. This configuration agrees with the magnetic configuration determined below 67 K from neutron diffraction experiments.[38] After optimizing the crystal structure at different pressure, band structures, and electronic densities of states have been calculated. We have also determined the complex dielectric function which has been used to calculate the absorption coefficient by means of the Kramers−Kronig relationship.[39]

3. RESULTS AND DISCUSSIONS

3.1. XRD Experiments. In Figure 1a, we present a selection of XRD patterns measured at different pressures. In agreement with ref 10, we have found that $NiWO_4$ does not undergo any phase transition in the pressure range covered by our studies, i.e., the crystal structure can be described as isomorphic to wolframite up to 20 GPa. This is supported by the results of Rietveld refinements shown in Figure 1a at 1.5 and 18.7 GPa. The goodness-of-fit parameters are R_p = 3.46% and R_{wp} = 5.38% at 1.5 GPa (R_p = 7.42% and R_{wp} = 10.53% at 18.7 GPa). The broadening of peaks observed at 18.7 GPa is a consequence of the solidification of the pressure medium at 10 GPa and the consequent increase of pressure gradients across the pressure chamber.[22] The observed peak broadening is typical in experiments performed using 16:3:1 MEW as pressure-medium and has also been observed in ref 10.

From the structural refinements, we have obtained the pressure dependence of unit-cell parameters. The results are shown in Figure 1b−d. In the figures, we compare the results of our experiments with the previous experiments[10] and our DFT calculations. All results show a similar pressure dependence with the calculations slightly overestimating the value of the β angle. Interestingly the previous experiments[10] show an abrupt decrease of the volume compressibility around 7 GPa. This phenomenon is not observed in our experiments and calculations. The change of compressibility could not be related to non-hydrostatic effects because the present and the previous experiment were performed using the same pressure medium, which is quasi-hydrostatic up to 10 GPa. We think the change of compressibility might be related to sample bridging between diamonds, which could strongly affect the compressibility of the sample.[40]

We have used a third-order Birch−Murnaghan equation of state[41] to fit the pressure dependence of the volume obtained from our experiments. The zero-pressure volume (V_0), bulk modulus (K_0), and its pressure derivative (K_0') we have determined are V_0 = 128.0(3) Å^3, K_0 = 137(17) GPa, and K_0' = 5.5(2.3). From our calculations we have obtained V_0 = 129.12(1) Å^3, K_0 = 147.4(6) GPa, and K_0' = 5.38(8). The values of K_0 and K_0' obtained from our experiments and calculations agree within uncertainties, which shows that calculations accurately describe the changes induced by pressure in the crystal structure. In the previous study,[10] it was reported that according to experiments, V_0 = 129.12(1) Å^3, K_0 = 146.05(2) GPa, and K_0' = 14.40(1). We consider that the overestimation of the pressure derivative of the bulk modulus is an artifact caused by the abrupt change of compressibility that occurs in previous experiments at 7 GPa.[10] From previous calculations, it was reported that V_0 = 133.16(8) Å^3, K_0 = 162.91(2) GPa, and K_0' = 3.64(2). The bulk modulus is larger than in our present results, but the pressure derivative is smaller. Thus, since both parameters are correlated,[42] it is not obvious to compare results from previous calculations and the previous study. To do it, we have refitted the results of previous calculations, but fixing K_0' = 5.38, the values obtained from our calculations. This way we have obtained V_0 = 133.39(8) Å^3 and K_0 = 147.3(1.5) GPa in excellent agreement with our results. Therefore, we are confident that the bulk modulus of $NiWO_4$ is 137−147 GPa, and its pressure derivative is 5.4−5.5.

From Figure 1b, it can be seen that the compressibility of $NiWO_4$ is slightly anisotropic. Since the crystal structure is monoclinic, the analysis of compressibility is not straightforward and requires the use of the compressibility tensor, which has four elements different than zero,[43] and the determination of its eigenvalues and eigenvectors. We have obtained them using PASCal.[44] We have found that the main axes of compressibility are (010), $(\bar{8}09)$, and (806). The corresponding linear compressibilities are 2.6(1) × 10^{-3} GPa, 2.0(2) × 10^{-3} GPa, and 1.3(1) × 10^{-3} GPa, respectively. As in other wolframites, the most compressible axis is the *b*-axis. The other two axes have similar compressibilities. They are in the plane perpendicular to the *b*-axis making an angle of 86° between them.

https://doi.org/10.1021/acs.jpcc.3c03512
J. Phys. Chem. C 2023, 127, 15630−15640

3.2. Optical-Absorption Experiments. In Figure 2a, we show the results of our optical-absorption measurements at different pressures. At 0 GPa, there is a sharp absorption at high-energy that corresponds to the fundamental band gap and five absorption bands that correspond to sub-gap Ni^{2+} $d-d$ internal transitions which are identified as E_i (i = 1−5). As pressure increases, the band gap red-shifts (see Figure 2a) and four of the Ni^{2+} $d-d$ bands blue-shift, while the fifth one does not move with pressure. Consequently, the Ni^{2+} $d-d$ band which is at 2.7 eV at 0 GPa moves into the fundamental band gap. To determine the band-gap energy, we have used a Tauc plot[45] assuming an indirect band gap (as supported by our DFT calculations which are reported at the end of this subsection). In this method, the band-gap energy is determined from the extrapolation to the abscissa of the linear region of $(E\alpha)^{1/2}$ versus energy (see Figure 2a). Readers should be aware that this energy should be considered as a lower bound for the band-gap energy.[46] As it can be seen in the inset of Figure 2a, the band-gap energy at 0 GPa is estimated to be 3.00(5) eV. Comparing with previous experiments,[10,12−18] our band-gap energy best agrees with the result reported by Ye et al.[9] From our experiments, we have determined the pressure dependence of the band-gap energy (E_{gap}) which is shown in Figure 2b. The pressure dependence of E_{gap} can be well described by a linear function as shown with a red solid line in Figure 2b. The pressure coefficient of this function, dE_{gap}/dP, is −13(1) meV/GPa, which is in excellent agreement with previous results.[10] The pressure dependence obtained from experiments also agrees with that obtained from our calculations (see Figure 2b).

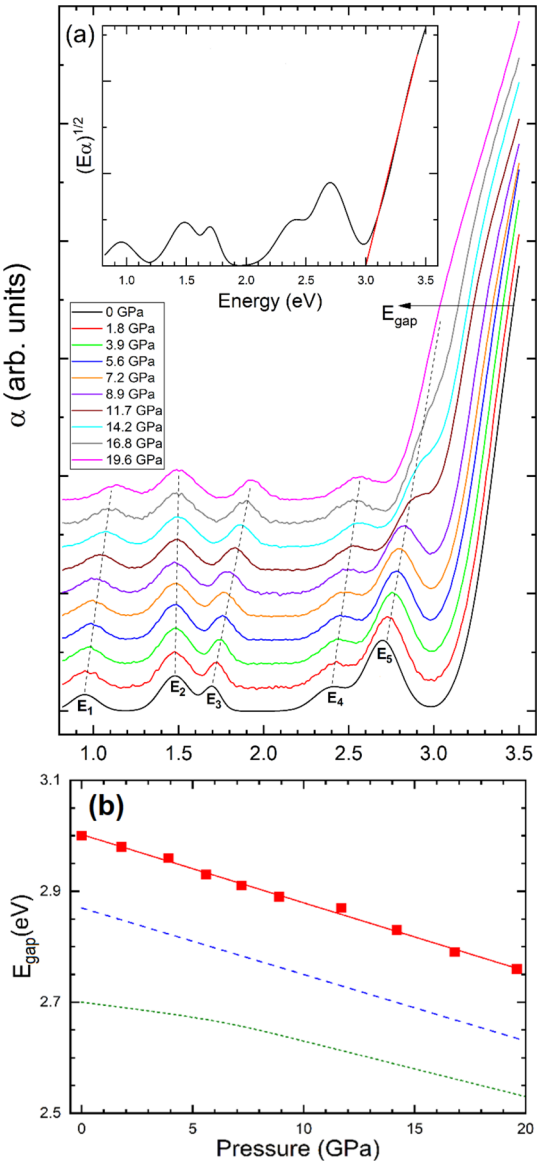

Figure 2. (a) Absorbance (α) of $NiWO_4$ at different pressures. The spectra have been offset vertically to make their identification easier. The assignment for the sub-gap bands is provided at 0 GPa. The dashed lines follow the sub-gap bands with pressure increase. The inset shows the Tauc plot at 0 GPa with the solid line used to determine the band-gap energy, E_{gap} = 3.0 eV. (b) E_{gap} determined from experiments (symbols), present calculations (dotted line), and from ref 10 (dashed line). The red solid line is a linear fit to experiments.

From the experiments, we could also follow the pressure dependence of Ni^{2+} $d-d$ transitions (see dashed lines in Figure 2a). The results are shown in Figure 3a. We have determined the pressure dependence for the five Ni^{2+} $d-d$ bands. In ref 10, only the pressure dependence of bands here labeled as E_3 and E_5 was reported. For these two bands, we observed the same

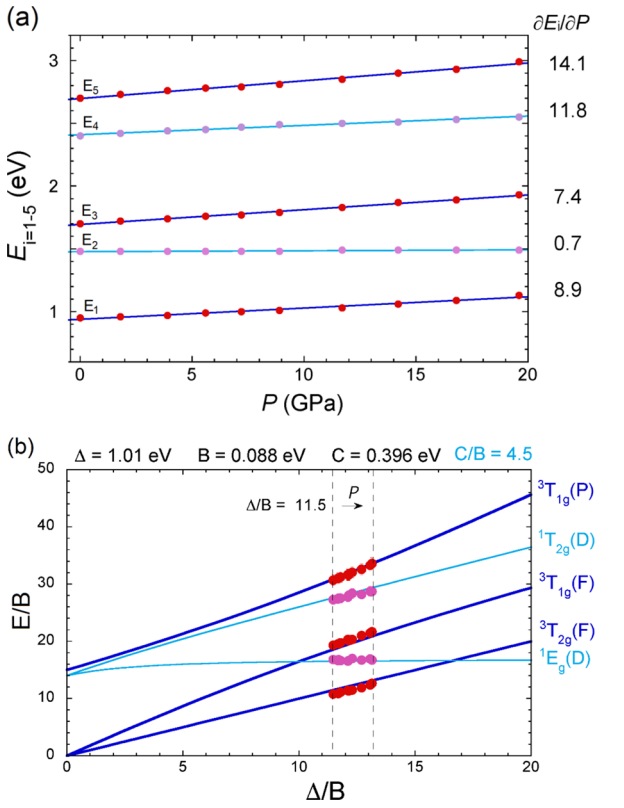

Figure 3. (a) Pressure dependence of the energy of Ni^{2+} $d-d$ transitions. Symbols are from the present experiment. The solid lines are from present pressure fits collected in Table 1. The pressure shift of each band is given right side in meV/GPa units. (b) Tanabe−Sugano (TS) diagram used for the interpretation of experiments showing the variation of the crystal-field transition energies, E/B, as a function of Δ/B within the d^8 configuration of Ni^{2+}. Circles are experimental data obtained at different pressures. In both figures, dark blue and cyan curves represent results for the spin-allowed transitions and for transition with spin change, respectively.

https://doi.org/10.1021/acs.jpcc.3c03512
J. Phys. Chem. C 2023, 127, 15630−15640

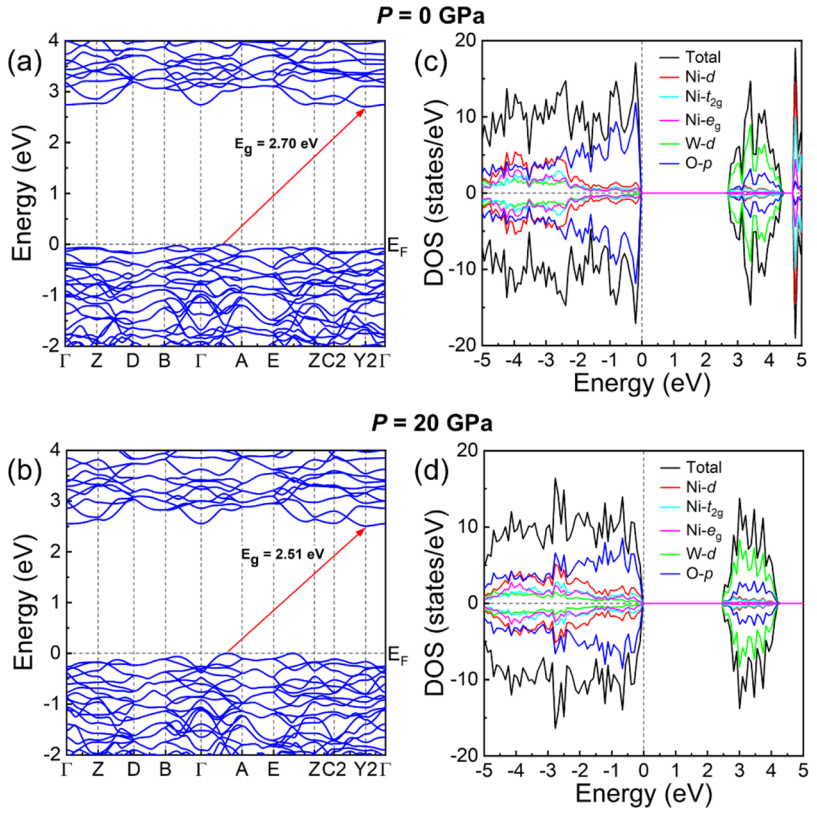

Figure 4. (a) Band structure at 0 GPa. (b) Band structure at 20 GPa. (c) Electron density of states at 0 GPa. (d) Electron density of states at 20 GPa.

linear increase of the energy with pressure. In our case, we obtained dE_5/dP = 14.8 meV/GPa and dE_3/dP = 11.8 meV/GPa, while the values reported for the pressure coefficients in ref 10 are 14.8 and 7.4 meV/GPa, respectively. In Figure 3a, it can be also seen than E_1 and E_4 increase under compression, whereas E_2 is not affected by pressure. A detailed behavior of the pressure dependence of Ni^{2+} $d-d$ transitions will be discussed in the next section.

Interestingly, in $NiWO_4$, the band gap closes under compression as observed in isomorphic $MnWO_4$,[6] $CoWO_4$,[7] and $CuWO_4$.[8] On the other hand, this behavior is the opposite to what happens in wolframite-type $CdWO_4$, $ZnWO_4$, and $MgWO_4$[6] in which the band gap opens under compression. This latter behavior is a result of the increase of the crystal field (CF) which enhances the splitting between the top of the valence band and the bottom of the conduction band which are dominated by O *2p* states and W *5d* states. As in $MnWO_4$, $CoWO_4$, and $CuWO_4$, it is possible that the closing under pressure of the band gap in $NiWO_4$ could be related to the contribution of Ni *3d* states to the top of the valence band or the bottom of the conduction band. This hypothesis is supported by our DFT calculations as we will show next.

In Figure 4, we show the calculated band structure (4a and 4b) and electron density of states (4c and 4d) at 0 and 20 GPa. Previous calculations gave a band-gap energy of 2.1 eV[10] and 3.91 eV[47] at 0 GPa. Our calculations give a band-gap energy of 2.7 eV, which is much closer to the experimental value. Calculations by Ye et al.[10] might have underestimated the band gap because they consider a non-magnetic configuration and/or used a Hubbard parameter U = 3.2 eV for Ni. We carried out simulations for the magnetic stable configuration using the same Hubbard parameter and obtained a band-gap energy of 2.07 eV showing that the problem of previous calculations was mainly the choice of the Hubbard parameter. On the other hand, Rosal et al.[47] performed calculations using the Becke 3-paramters Lee−Yang−Parr (B3LYP) hybrid functional[48] assuming a non-magnetic configuration and ignoring the Hubbard term. In the Supplementary Material of their work, it can be seen that this approach does not describe as accurately as our calculations the crystal structure of $NiWO_4$ at 0 GPa. Thus, it is not surprising that their DFT approach leads to an overestimated band-gap energy.

The band structure at 0 and 20 GPa is represented in Figure 4a,b. The electron density of states at 0 and 20 GPa is represented in Figure 4c,d. We have also calculated the absorption coefficient which is shown in Figure 5. Figure 4 shows that $NiWO_4$ is an indirect band gap semiconductor and

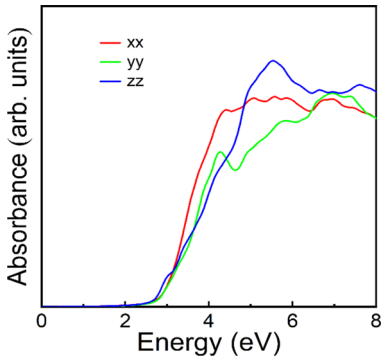

Figure 5. Calculated absorbance spectrum at 0 GPa for different polarizations.

https://doi.org/10.1021/acs.jpcc.3c03512
J. Phys. Chem. C 2023, 127, 15630−15640

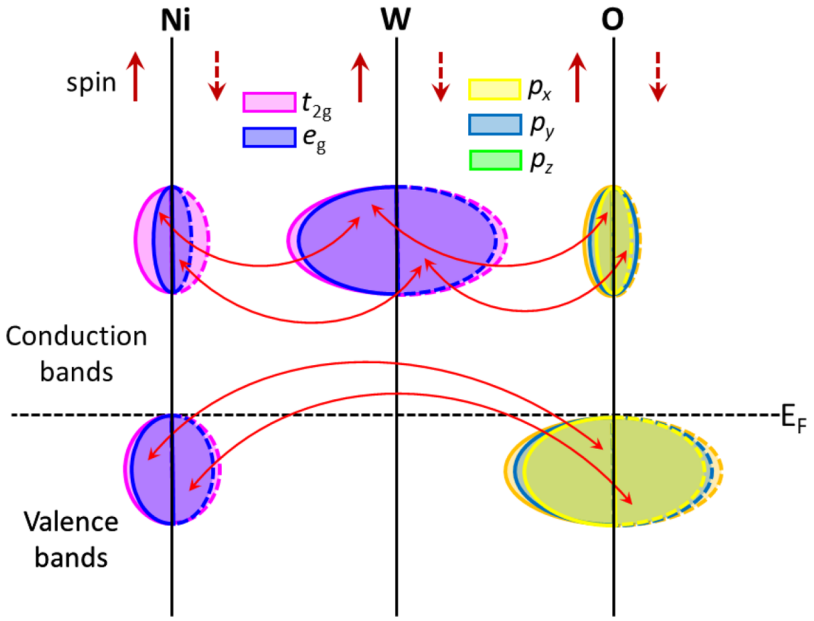

Figure 6. Schematic representation of the electronic density of states of $NiWO_4$ around the Fermi level.

that the top of the valence is dominated by O *2p* states with a minor contribution from Ni *3d* states. Contrastingly, the bottom of the conduction band is dominated by W *5d* states. A schematic representation of the electronic density of states around the Fermi energy is shown in Figure 6. As expected for a compound with a conduction band with *d* character, the conduction is not very dispersive, and its energy minimum is not in the zone center being at the Y2 point of the Brillouin zone (see Figure 4a). On the other hand, the top of the valence band is at a point near the A point in the Brillouin zone. Regarding the absorption-coefficient, calculations show that $NiWO_4$ has an abrupt absorption starting at 2.7 eV (see Figure 5), which agrees with the sharp absorption edge found in the experiments performed by Ejima et al. at 3.0 eV. Indeed, the shape of measured and calculated absorption is qualitatively similar. However, calculations do not predict the sub-bandgap Ni^{2+} *d*−*d* transitions because they are not accounted by the electric dipole approximation. In order to accurately calculate *d*−*d* transitions occurring below the band gap, it may be necessary to employ alternative methodologies that go beyond the electric dipole approximation. For example, methods such as time-dependent DFT or more advanced approaches like many-body perturbation theory (MBPT) can be utilized. These methods are capable of considering higher-order effects and providing a more precise description of the *d*−*d* transitions occurring below the bandgap.[49,50] Such calculations are beyond the scope of the present work.

Regarding pressure effects on the band structure, Figure 4b shows that at 20 GPa, the topology of the band structure has not changed significantly from 0 GPa (Figure 4a). However, though the bottom of the conduction band goes down with pressure, the top of the valence band remains at the same energy due to the increase of the contribution of Ni *3d* states to it. This is translated into the band-gap energy decrease we have observed in experiments. This behavior in $NiWO_4$ is qualitatively like those previously reported $MnWO_4$[6] and $CoWO_4$[7] as the contribution to band-gap energy in these compounds is also due to the contribution of *3d* states of Mn and Co near the Fermi level.

3.3. Ni^{2+} *d*−*d* Transitions. The origin of the sub-band-gap absorption features in $NiWO_4$ has been controversial and still deserves clarification.[10,12,13,49] So far, all papers dealing with the optical properties of $NiWO_4$ have reported different origins or misinterpretations of the sub-band-gap bands as Ni^{2+} CF transitions, defect related absorption, or excitonic components of the gap. Lima et al.[51] as well as Ye et al.[10] assigned bands at 1.68 and 2.73 eV to spin forbidden CF transitions from $^3A_{2g}$ to ^1E_g and $^1T_{2g}$, respectively. In contrast, Ejima et al.,[12] who reported energies similar to ours, assigned these bands to spin-allowed CF transitions with $^3T_1$ symmetry after comparison with the assignment given for $[Ni(H_2O)_6]^{2+}$ and NiO.[52] Ye et al.[10] attributed the band at 2.74 eV to an exciton associated with the band gap and the band at 1.48 eV, which does not move with pressure, to "the presence of Frenkel defects with the dislocation of Ni^{2+} from the octahedron to the tetrahedron site." On the other hand, de Oliveira et al.[13] assigned a shoulder at ∼2.7 eV as probably due to the presence of a midgap defect state. In all cases, the pressure experiments associated with the sub-band-gap spectra lack absorption bands, or they are poorly resolved by reflectometry measurements on $NiWO_4$ powders, making a proper band assignment difficult. In this context, HP measurements are important because the associated pressure shifts provide critical information for a proper band assignment. In this work, we have used a $NiWO_4$ sample sintered at HP using a DAC. This method provides a transparent parallelepipedal sample to perform suitable optical-absorption measurements at ambient conditions and as a function of pressure, which was crucial to achieve this goal.

The room-temperature optical absorption sub-gap spectrum of $NiWO_4$ shows five absorption bands, named E_i, at 0.95, 1.48, 1.70, 2.40, and 2.70 eV from i = 1 to 5, respectively. These five bands are also observed as main absorption features in the CF spectra of Ni^{2+} in oxides, fluorides, and chlorides,[52−57] as well as in $NiWO_4$.[12] The proposed band assignment to electronic CF transitions within the $3d^8$ configuration of Ni^{2+} is given in Figure 3b. Peak labels have been assigned according to the sixfold O_h symmetry of the

https://doi.org/10.1021/acs.jpcc.3c03512
J. Phys. Chem. C 2023, 127, 15630−15640

NiO_6 local environment of Ni^{2+}. Although the actual local symmetry around Ni^{2+} is slightly distorted with respect to O_h, the CF transition energies as well as their pressure dependence are well described on the basis of the TS diagram for d^8[58,59] (See Figure 3b). The energy of the five measured bands and their different pressure shifts were crucial for a correct band assignment. The Supplemental Material collects the measured transition energies at each pressure and the corresponding calculated energies as a function of the Racah parameters B and C and the CF energy Δ (=$10Dq$) of the 3d-orbitals split into e_g + t_{2g}. The assignment and CF parameters are similar to those originally given elsewhere[53−57] (See Figure S1). Therefore, the sub-gap bands correspond to intra-configurational CF transitions within the $3d^8$ configuration from the $^3A_{2g}(F)$ $[t_{2g}^6\ e_g^2]$ ground state to the excited states $^3T_{2g}(F)$, $^3T_{1g,a}(F)$, $^1E_g(D)$, $^1T_{2g}(D)$, and $^3T_{1g,a}(P)$, in order of increasing energy, in the low CF limit ($\Delta/B < 10$). However, the $^3T_{1g,a}(F)$ state energy exceeds the $^1E_g(D)$ energy for ($\Delta/B > 10$). Their transition energy as a function of B and C and Δ (see Figure 3b) is given by[58,59]

$$E_1 = E(^3T_{2g}(F)) = \Delta = 10Dq$$

$$E_3 = E(^3T_{1g}(F)) = \frac{15}{2}B + \frac{3}{2}\Delta - \sqrt{\left(\frac{\Delta}{2}\right)^2 + \left(\frac{15}{2}B\right)^2 - \frac{9}{2}B\Delta}$$

$$E_5 = E(^3T_{1g}(P)) = \frac{15}{2}B + \frac{3}{2}\Delta + \sqrt{\left(\frac{\Delta}{2}\right)^2 + \left(\frac{15}{2}B\right)^2 - \frac{9}{2}B\Delta} \quad (1)$$

for the spin-allowed transitions, and by

$$E_2 = E(^1E_g(D)) = \frac{17}{2}B + 2C + \Delta - \sqrt{\Delta^2 + \left(\frac{7}{2}B\right)^2 + B\Delta}$$

$$E_4 = E(^1T_{2g}(D)) = \frac{17}{2}B + 2C + \frac{3}{2}\Delta - \sqrt{\left(\frac{\Delta}{2}\right)^2 + \left(\frac{7}{2}\right)^2 + \frac{1}{2}B\Delta} \quad (2)$$

for transitions with spin change.

In particular, the energy of the $^3A_{2g}(F) \rightarrow {}^1E_g(D)$, E_2, is practically independent of Δ for $\Delta/B > 5$. The TS for Ni^{2+} as a plot of E/B vs Δ/B can be obtained directly from eqs 1 and 2 for a given C/B ratio. The energy of the $^3A_{2g}(F) \rightarrow {}^1E_g(D)$ transition, which corresponds to a spin-flip transition within the $t_{2g}^6e_g^2$ configuration, runs parallel to the Δ/B abscissa axis in the TS diagram for about $\Delta/B > 5$ (Figure 3b). The parameters B and Δ at ambient pressure were obtained by least-squares fitting of the experimental energies E_1, E_3, and E_5, whose energies depend on B and Δ but not on C, to eq 1. On the other hand, the spin-flip transition energies E_2 and E_4, which both depend on B, C, and Δ, were used to determine the parameter C from eq 2. The TS diagram of Figure 3b shows the experimental CF transition energies of the $NiWO_4$ absorption spectrum and the calculated ones using B = 0.088 eV, Δ = 1.01 eV; C/B = 4.5 (Δ/B = 11.5). Comparisons between measured and calculated energies at ambient pressure and as a function of pressure are collected in Table S1 at SI. It should be noted that the values obtained for B, C, and Δ at ambient pressure are somewhat unusual compared to other oxides and fluorides.[53−57] For example, the spectrum of $NiWO_4$ looks similar to the Ni^{2+} in MgO (bunsenite) or NiO (periclase) where energies of the spin-allowed transitions appear at 1.07 eV ($^3T_{2g}(F)$), 1.67 eV ($^3T_{1g}(F)$), and 3.05 eV ($^3T_{1g}(P)$); and 1.09, 1.75 and 2.99 eV, respectively;[53,54] or 0.91, 1.55, and 2.95 eV in $KNiF_3$.[55] It must be noted that the separation between the experimental $^4T_{1g}$ energies, E = $E(^3T_{1g}(P))$- $E(^3T_{1g}(F))$ = $E_5 - E_3$, which has values of 1.38 eV for MgO, 1.24 eV for NiO, and 1.40 eV for $KNiF_3$, is only of 1.0 eV for $NiWO_4$ having a similar Δ value. This relatively smaller energy difference between E_5 and E_3 reflects the lower value of the measured CF splitting Δ = 0.95 eV as compared to that obtained by fitting Δ = 1.01 eV (about 6%). The opposite trend is observed for E_3 (see Table S1 in Supplementary Material).

An examination of the optical absorption of $NiWO_4$ at ambient pressure suggests that the second band E_2 could initially be assigned to $^3T_{1g}(F)$ and the third band E_3 to $^1E_g(D)$. In fact, such an assignment is in better agreement with the transition energies of other Ni^{2+} compounds with CF splitting lower than 1.0 eV (E_1 < 1.0 eV) such as $KNiF_3$[54] than with Ni^{2+} oxides with CF values of about 1.2 eV (E_1 > 1.0 eV) obtained in NiO and other oxides.[53−55] In addition, the assignment of E_3 to $^1E_g(D)$ would be supported by the fact that its intensity is lower than E_2 as it would be expected for a spin-flip transition such as $^1E_g(D)$ as opposed to a spin-allowed transition such as $^3T_{1g}(F)$. The assignment given elsewhere[10,51] is consistent with this interpretation. However, the fact that we are close to the crossover of the $^3T_{1g}(F)$-$^1E_g(D)$ states around Δ/B = 10 makes the band assignment more complicated. Under such circumstances, the Fano resonance induced by the spin-orbit coupling interaction at the crossover point can equal their respective absorption coefficient, as occurs at the $^4T_{2g} - {}^2E_g$ crossover point in Cr^{3+}.[60] Furthermore, the electric-dipole exchange-induced mechanism, which is very active in exchange-coupled Ni^{2+} pairs or concentrated materials,[56,57] can modify the absorption intensities of spin-flip transitions.

Pressure measurements definitely clarify the band assignment based on the pressure shifts. Besides the transition energies E_i, the pressure derivatives $\frac{\partial E_i}{\partial P}$ are very different for E_2 and E_3 as it is shown in the TS diagram of Figure 3b. Furthermore, we can directly compare the measured pressure shifts $\frac{\partial E_i}{\partial P}$ and the calculated CF-derivatives of E_i $\frac{\partial E_i}{\partial \Delta}$, as derived from eqs 1 and 2. These two derivatives are related by the pressure derivative of the CF, $\frac{\partial \Delta}{\partial P}$, which for Ni^{2+} coincides with the pressure derivative of the first band: $\frac{\partial E_1}{\partial P} = \frac{\partial \Delta}{\partial P}$.

Therefore, $\frac{\partial E_i}{\partial P}$ and $\frac{\partial E_i}{\partial \Delta}$ are related by the expression: $\frac{\partial E_i}{\partial P} = \frac{\partial E_i}{\partial \Delta}\frac{\partial \Delta}{\partial P} = \frac{\partial E_i}{\partial \Delta}\frac{\partial E_1}{\partial P}$. So that, the experimental variation $\left(\frac{\partial E_i}{\partial \Delta}\right)_{exp}$ can be obtained from the pressure shifts through the expression: $\left(\frac{\partial E_i}{\partial \Delta}\right)_{exp} = \frac{\left(\frac{\partial E_i}{\partial P}\right)_{exp}}{\left(\frac{\partial E_1}{\partial P}\right)_{exp}}$.

The variations $E_i(P)$ are shown in Figure 3a together with their respective pressure derivative $\left(\frac{\partial E_i}{\partial P}\right)_{exp}$. Table 1 compares

https://doi.org/10.1021/acs.jpcc.3c03512
J. Phys. Chem. C 2023, 127, 15630−15640

Table 1. Transition Energies and Corresponding Pressure Shifts of the Five Sub-Gap Bands E_i (i = 1−5) of $NiWO_4$ at Ambient Pressure[a]

transition energy	E_1	E_2	E_3	E_4	E_5
band assignment $^3A_{2g}(F)\rightarrow$	$^3T_{2g}(F)$	$^1E_g(D)$	$^3T_{1g}(F)$	$^1T_{2g}(D)$	$^3T_{1g}(P)$
experimental E_i (P = 0; eV)	0.95	1.48	1.70	2.40	2.70
experimental $\frac{\partial E_i}{\partial P}$ (meV GPa^{-1})	8.9	0.7	11.8	7.4	14.1
experimental $\frac{\partial E_i}{\partial \Delta} = \frac{\left(\frac{\partial E_i}{\partial P}\right)}{\left(\frac{\partial E_1(=\Delta)}{\partial P}\right)}$	1.0	0.08	1.33	0.83	1.62
calculated from TS $\frac{\partial E_i}{\partial \Delta}$	1.0	0.04	1.40	1.07	1.60

[a]The proposed band assignment to crystal-field transitions within the $3d^8$ configuration of Ni^{2+} is included. The comparison between experimental and calculated crystal-field derivatives of the transition energies are shown in last two rows. The crystal-field derivatives were calculated from eqs 1 and 2 for Δ/B = 11.5.

the experimental pressure derivatives $\left(\frac{\partial E_i}{\partial \Delta}\right)_{exp}$ with the calculated ones $\left(\frac{\partial E_i}{\partial \Delta}\right)_{calc}$ from eqs 1 and 2 for Δ/B = 11.5. It turns out that, as in most oxides, the energy of the CF-independent spin-flip transition $^1E_g(D)$ corresponds to E_2, while $^3T_{1g}(F)$ to E_3. The assignment of E_1, E_4, and E_5 to $^3T_{2g}(F)$, $^1T_{2g}(D)$ and $^3T_{1g}(P)$, respectively, is consistent with both their energy and CF-derivative, thus clarifying the origin of the present sub-gap bands in $NiWO_4$. Figure 3b shows the TS diagram and the measured energies with respect to the B parameter. The agreement between the measured and calculated energies with Δ/B is fully consistent with the proposed band assignment.

The present work also provides the dependence of the CF splitting Δ with the crystal volume through $V(P)$ and $B(P)$. Figure 7 shows the variation of the CF splitting with V and the inset is the variation $B(P)$ in the studied pressure range. An important conclusion is that, within the accuracy of the data, parameter B can be considered as B = 0.088 eV in the range 0−20 GPa. In fact, B changes only 0.8 meV (from 0.0882 to 0.0890 eV) in this pressure range. In contrast, the variation $\Delta(P)$ as 8.9 meVGPa^{-1} is plotted as a function of the volume and gives an exponent in the variation $\Delta = \Delta_0\left(\frac{V_0}{V}\right)^{n/3}$ as n = 3.8(4). This value is smaller than the CF estimates n = 5 for an O_h symmetry and what has been found for other divalent transition-metal ions in oxides[61] and even fluorides.[55,62] The low local symmetry of Ni^{2+} in $NiWO_4$ can probably account for the different n exponent compared to compounds containing the transition-metal ions in O_h sites.

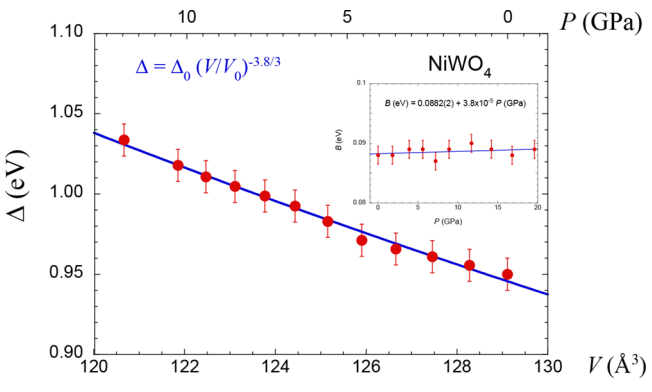

Figure 7. Variation of the CF splitting $\Delta(P)$ with the crystal volume V using the $V(P)$ data of Figure 1b. The $\Delta(V)$ data have been fitted to the equation $\Delta = \Delta_0\left(\frac{V_0}{V}\right)^{n/3}$ with fit parameters of n = 3.8(4), Δ_0= 0.946(2) eV, and V_0= 129.1(2) Å^3. The inset is the variation $B(P)$ in the explored pressure range. Within the data accuracy, B = 0.088 eV as it changes from 0.0882 to 0.0890 eV in the 0−20 GPa range. We obtain that C/B = 4.5 in this pressure range.

3.4. Resistivity and Hall-Effect Experiments. To conclude, we will present results we obtained for electrical transport properties. Our Hall-effect measurements indicate that $NiWO_4$ behaves as a p-type semiconductor. This could be related with the presence of acceptor levels associated with the presence of Ni vacancies.[63] Figure 8 shows the pressure dependence of the resistivity (ρ), carrier concentration (p), and mobility (μ) up to 10 GPa. The resistivity at 0 GPa is comparable with that reported by Bharati et al.[64] from experiments performed in single crystals. In the past, it was proposed that electrical conductivity can be related to the transfer of d-electrons between neighboring metal ions and by

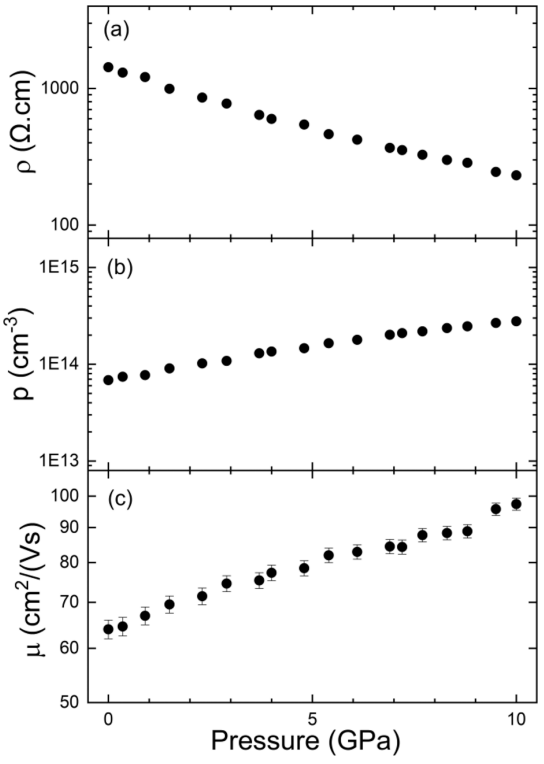

Figure 8. (a) Resistivity, (b) carrier concentration, and (c) carrier mobility of $NiWO_4$ versus pressure.

https://doi.org/10.1021/acs.jpcc.3c03512
J. Phys. Chem. C 2023, 127, 15630−15640

exciting electrons from the valence bands to the conduction bands. However, the carrier concentration we measured is more consistent with an extrinsic semiconductor in which related acceptor levels can be caused by a small concentration of Ni vacancies as recently reported in nickel oxide.[63] Under compression, we found that the resistivity decreases. This is a consequence of both the increase of the carrier concentration and mobility. The increase of the carrier mobility could be related to a decrease of the effective mass of holes, which is consistent with the increase of the convexity of the valence band around the maximum as pressure increases (see Figure 4a,b). On the other hand, assuming the semiconductor is extrinsic, from the pressure dependence of the carrier concentration, we can obtain how the activation energy of donors changes with pressure. From our results, we obtain the activation energy decreases with pressure at a rate of −3.6(3) meV/GPa. Such pressure dependence is comparable to that reported for shallow acceptors in other *p*-type semiconductors.[65,66] Thus, the presence of acceptors associated with nickel vacancies in $NiWO_4$ provides a reasonable hypothesis to explain our transport measurements at ambient and high pressure.

4. CONCLUSIONS

From powder XRD experiments, we determined the changes induced by pressure in the crystal structure of $NiWO_4$. We confirmed that it does not undergo any phase transition up to 20 GPa and determined its bulk modulus, main axes of compressibility, and linear compressibility of these axes. We also determined that $NiWO_4$ has a band-gap energy of 3.0 eV which decreases with a pressure coefficient of −13(1) meV/GPa. Both conclusions are supported by DFT calculations which provide a rationale for the changes induced by pressure in the band-gap energy. In particular, calculations show that Ni *3d* electrons play a crucial role in the closing of the band gap. We also demonstrated that the five sub-gap bands of $NiWO_4$ correspond to crystal-field transitions within the $3d^8$ (t_{2g}^6 e_g^2) configuration of Ni^{2+} and clarified their assignment based on their respective energy and pressure shifts. In particular, the different pressure shifts of bands E_2 (0.7 meVGPa^{-1}) and E_3 (11.8 meVGPa^{-1}) allowed us to unravel their origin as CF transitions to the $^1E_g(D)$ and $^3T_{1g}(F)$ states, respectively, thus resolving a controversial issue in $NiWO_4$. Both the energy and pressure dependence were well described on the basis of the semiempirical CF theory using the Tanabe−Sugano method. Finally, resistivity and Hall-effect measurements showed that $NiWO_4$ is a *p*-type semiconductor in which the resistivity decreases under compression due to the increase of both the carrier concentration and mobility. This implies that thin films of $NiWO_4$ under compressive stress can prove to be better electrode materials for supercapacitors.

■ ASSOCIATED CONTENT

Data Availability Statement

The data that support the findings of this study are available from the corresponding author upon reasonable request.

Supporting Information

The Supporting Information is available free of charge at https://pubs.acs.org/doi/10.1021/acs.jpcc.3c03512.

Comparisons between measured and calculated energies at ambient pressure and as a function of pressure (PDF)

■ AUTHOR INFORMATION

Corresponding Authors

Daniel Errandonea − *Departamento de Física Aplicada-ICMUV, MALTA Consolider Team, Universidad de Valencia, 46100 Valencia, Spain;* orcid.org/0000-0003-0189-4221; Email: daniel.errandonea@uv.es

Ganapathy Vaitheeswaran − *School of Physics, University of Hyderabad, Hyderabad 500 046 Telangana, India;* orcid.org/0000-0002-2320-7667; Email: vaithee@uohyd.ac.in

Authors

Fernando Rodriguez − *DCITIMAC, MALTA Consolider Team, Facultad de Ciencias, Universidad de Cantabria, 39005 Santander, Spain*

Rosario Vilaplana − *Centro de Tecnologías Físicas, Universitat Politècnica de València, 46022 Valencia, Spain;* orcid.org/0000-0003-0504-2157

David Vie − *Institut de Ciència dels Materials de la Universitat de València, E-46071 València, Spain*

Siddhi Garg − *High-Pressure and Synchrotron Radiation Physics Division, Bhabha Atomic Research Centre, Trombay, Mumbai 400085, India;* orcid.org/0009-0005-1529-4384

Bishnupriya Nayak − *High-Pressure and Synchrotron Radiation Physics Division, Bhabha Atomic Research Centre, Trombay, Mumbai 400085, India*

Nandini Garg − *High-Pressure and Synchrotron Radiation Physics Division, Bhabha Atomic Research Centre, Trombay, Mumbai 400085, India; Homi Bhabha National Institute, Anushaktinagar, Mumbai 400094, India*

Jaspreet Singh − *Department of Physics, Indian Institute of Technology Hyderabad, 502284 Sangareddy, Telangana, India*

Venkatakrishnan Kanchana − *Department of Physics, Indian Institute of Technology Hyderabad, 502284 Sangareddy, Telangana, India;* orcid.org/0000-0003-1575-9936

Complete contact information is available at: https://pubs.acs.org/10.1021/acs.jpcc.3c03512

Author Contributions

D.E. conceived the project. R.V. and D.V. synthesized and characterized the sample. S.G., B.N., and N.G. performed powder XRD experiments. D.E. performed optical and transport experiments, D.E., F.R., and R.V. performed data analysis. J.S., V.K., and G.V. performed density-functional theory calculations. D.E., F.R., N.G., and G.V. contributed to discussions. All authors participated in writing and editing of the manuscript. All authors have given approval to the final version of the manuscript.

Notes

The authors declare no competing financial interest.

■ ACKNOWLEDGMENTS

D.E. acknowledges the financial support from the Generalitat Valenciana under grant nos. PROMETEO CIPROM/2021/075-GREENMAT and MFA/2022/007 and Spanish Ministerio de Ciencia e Innovación and Agencia Estatal de Investigación (MCIN/AEI/10.13039/501100011033) and the European Union under grant nos. PID2019-106383GB-41/42 and RED2018-102612-T (MALTA Consolider-Team network). This study forms part of the Advanced Materials

program and is supported by MCIN with funding from European Union Next Generation EU (PRTR-C17.I1) and by the Generalitat Valenciana. F.R. acknowledges financial support from Projects PID2021-127656NB-I00 and MALTA-Consolider Team (RED2018-102612-T) from the State Research Agency of Spain, Ministry of Science and Innovation. The authors J.S. and V.K. would like to acknowledge IIT Hyderabad for computational facility. V.K. would like to acknowledge DST-FIST (SR/FST/PSI-215/2016) for the financial support. J.S. would like to acknowledge CSIR for the fellowship. G.V. would like to acknowledge Institute of Eminence, University of Hyderabad (UoH-IoE-RC3-21-046) for funding and CMSD University of Hyderabad for providing the computational facility. We thank Dr. Velaga Srihari and Smt. Vasanthi for helping with the data acquisition at BL11 beamline at INDUS2.

REFERENCES

(1) Shaheen, N.; Aadil, M.; Zulfiqar, S.; Sabeeh, H.; Agboola, P. O.; Warsi, M. F.; Aboud, M. F. A.; Shakir, I. Fabrication of different conductive matrix supported binary metal oxides for supercapacitors applications. *Ceram. Int.* **2021**, *47*, 5273−5285.
(2) Ji, Y.; Yang, L.; Ren, X.; Cui, G.; Xiong, X.; Sun, X. Full Water Splitting Electrocatalyzed by $NiWO_4$ Nanowire Array. *ACS Sustainable Chem. Eng.* **2018**, *6*, 9555−9559.
(3) Mikhailik, V. B.; Kraus, H. Performance of Scintillation Materials at Cryogenic Temperatures. *Phys. Status Solidi B* **2010**, *247*, 1583−1599.
(4) Keeling, R.O., Jr. The structure of $NiWO_4$. *Acta Crystallogr.* **1957**, *10*, 209−213.
(5) Cornelis, K.; Hurlbut, C.S., Jr. *Manual of Mineralogy*, 20th ed.; Wiley, 1985; pp 355−356.
(6) Errandonea, D.; Ruiz-Fuertes, J. A Brief Review of the Effects of Pressure on Wolframite-Type Oxides. *Crystals* **2018**, *8*, 71.
(7) Ruiz-Fuertes, J.; López-Moreno, S.; López-Solano, J.; Errandonea, D.; Segura, A.; Lacomba-Perales, R.; Mũnoz, A.; Radescu, S.; Rodríguez-Hernández, P.; Gospodinov, M.; Nagornaya, L. L.; Tu, C. Y. Pressure Effects on the Electronic and Optical Properties of AWO_4 Wolframites (A = Cd, Mg, Mn, and Zn): The Distinctive Behavior of Multiferroic $MnWO_4$. *Phys. Rev. B* **2012**, *86*, No. 125202.
(8) Bandiello, E.; Rodríguez-Hernández, P.; Muñoz, A.; Buenestado, M. B.; Popescu, C.; Errandonea, D. Electronic Properties and High-Pressure Behavior of Wolframite-Type $CoWO_4$. *Mater. Adv.* **2021**, *2*, 5955−5966.
(9) Ruiz-Fuertes, J.; Segura, A.; Rodríguez, F.; Errandonea, D.; Sanz-Ortiz, M. N. Anomalous High-Pressure Jahn-Teller Behavior in $CuWO_4$. *Phys. Rev. Lett.* **2012**, *108*, No. 166402.
(10) Ye, M.; Zhou, Y.; Shao, T.; Liu, H.; Tao, Q.; Wang, X.; Tang, R.; Yue, H.; Li, Y.; Zhu, P. Effects of High Pressure on the Bandgap and the d−d Crystal Field Transitions in Wolframite $NiWO_4$. *J. Phys. Chem. C* **2023**, *127*, 6543−6551.
(11) Liang, A.; Turnbull, R.; Errandonea, D. A review on the advancements in the characterization of the high-pressure properties of iodates. *Prog. Mater. Sci.* **2023**, *136*, No. 101092.
(12) Ejima, T.; Banse, T.; Takatsuka, H.; Kondo, Y.; Ishino, M.; Kimura, N.; Watanabe, M.; Matsubar, I. Microscopic optical and photoelectron measurements of MWO_4 (M= Mn, Fe, and Ni). *J. Lumin.* **2006**, *119−120*, 59−63.
(13) de Oliveira, A. L. M.; Ferreira, J. M.; Silva, M. R. S.; de Souza, S. C.; Vieira, F. T. G.; Longo, E.; Souza, A. G.; Santos, M. G. Influence of the thermal treatment in the crystallization of $NiWO_4$ and $ZnWO_4$. *J. Therm. Anal. Calorim.* **2009**, *97*, 167−172.
(14) Oliveira, Y. L.; Costa, M. J. S.; Juca, A. C. S.; Silva, L. K. R.; Longo, E.; Arul, N. S.; Cavalcante, L. S. Structural characterization, morphology, optical and colorimetric properties of $NiWO_4$ crystals synthesized by the co-precipitation and polymeric precursor methods. *J. Mol. Struct.* **2020**, *1221*, No. 128774.
(15) Bhattacharya, A. K.; Biswas, R. G.; Hartridge, A. Environment sensitive impedance spectroscopy and dc conductivity measurements on $NiWO_4$. *J. Mater. Sci.* **1997**, *32*, 353−356.
(16) Ahmed, M. I.; Adam, A.; Khan, A.; Siddiqui, M. N.; Yamani, Z. H.; Qamar, M. Q. Synthesis of mesoporous $NiWO_4$ nanocrystals for enhanced photo electrochemical water oxidation. *Mater. Lett.* **2016**, *177*, 135−138.
(17) Dridi, R.; Dridi, D.; Hammami, S.; Dimassi, W.; Chtourou, R.; Amlouk, M. Growth and physical investigations on $NiWO_4$ thin films as a potential for NO_2 sensing. *Optik* **2023**, *273*, No. 170330.
(18) Pandey, P. K.; Bhave, N. S.; Kharat, R. B. Structural, optical, electrical and photovoltaic electrochemical characterization of spray deposited $NiWO_4$ thin films. *Electrochim. Acta* **2006**, *51*, 4659−4664.
(19) AlShehri, S. M.; Ahmed, J.; Alzahrani, A. M.; Ahamad, T. Synthesis, characterization, and enhanced photocatalytic properties of $NiWO_4$ nanobricks. *New J. Chem.* **2017**, *41*, 8178−8186.
(20) Weitzel, H. Kristallstrukturverfeinerung von Wolframiten und Columbiten. *Z. Kristallogr. - Cryst. Mater.* **1976**, *144*, 238−258.
(21) Pandey, K. K.; Poswal, H. K.; Mishra, A. K.; Dwivedi, A.; Vasanthi, R.; Garg, N.; Sharma, S. M. Energy-dispersive X-ray diffraction beamline at Indus-2 synchrotron source. *Pramana* **2013**, *80*, 607−619.
(22) Klotz, S.; Chervin, J. C.; Munsch, P.; Le Marchand, G. Hydrostatic limits of 11 pressure transmitting media. *J. Phys. D: Appl. Phys.* **2009**, *42*, No. 075413.
(23) Dewaele, A.; Loubeyre, P.; Mezouar, M. Equations of state of six metals above 94 GPa. *Phys. Rev. B* **2004**, *70*, No. 094112.
(24) Prescher, C.; Prakapenka, V. B. DIOPTAS: a program for reduction of two-dimensional X-ray diffraction data and data exploration. *High Pressure Res.* **2015**, *35*, 223−230.
(25) Toby, B. H. EXPGUI, a graphical user interface for GSAS. *J. Appl. Crystallogr.* **2001**, *34*, 210−213.
(26) Mao, H. K.; Xu, J.; Bell, P. M. Calibration of the Ruby Pressure Gauge to 800 Kbar under Quasi-Hydrostatic Conditions. *J. Geophys. Res.* **1986**, *91*, 4673−4676.
(27) Errandonea, D.; Bandiello, E.; Segura, A.; Hamlin, J. J.; Maple, M. B.; Rodriguez-Hernandez, P.; Muñoz, A. Tuning the band gap of $PbCrO_4$ through high-pressure: Evidence of wide-to-narrow semiconductor transitions. *J. Alloys Compd.* **2014**, *587*, 14−20.
(28) Errandonea, D.; Segura, A.; Martínez-García, D.; Muñoz-San Jose, V. Hall-effect and resistivity measurements in CdTe and ZnTe at high pressure: Electronic structure of impurities in the zinc-blende phase and the semimetallic or metallic character of the high-pressure phases. *Phys. Rev. B* **2009**, *79*, No. 125203.
(29) Errandonea, D.; Martinez-Garcia, D.; Segura, A.; Ruiz-Fuertes, J.; Lacomba-Perales, R.; Fages, V.; Chevy, A.; Roa, L.; Muñoz, V. High-pressure electrical transport measurements on p-type GaSe and InSe. *High Pressure Res.* **2006**, *26*, 513−516.
(30) Kresse, G.; Furthmüller, J. Efficient iterative schemes for ab initio total-energy calculations using a plane-wave basis set. *Phys. Rev. B* **1996**, *54*, 11169−11186.
(31) Kresse, G.; Joubert, D. From ultrasoft pseudopotentials to the projector augmented-wave method. *Phys. Rev. B* **1999**, *59*, 1758−1775.
(32) Perdew, J. P.; Burke, K.; Ernzerhof, M. Generalized gradient approximation made simple. *Phys. Rev. Lett.* **1996**, *77*, 3865−3868.
(33) Blöchl, P. E. Projector augmented-wave method. *Phys. Rev. B* **1994**, *50*, 17953−17979.
(34) Monkhorst, H. J.; Pack, J. D. Special points for Brillouin-zone integrations. *Phys. Rev. B* **1976**, *13*, 5188−5192.
(35) Dudarev, S. L.; Botton, G. A.; Savrasov, S. Y.; Humphreys, C. J.; Sutton, A. P. Electron-energy-loss spectra and the structural stability of nickel oxide: An LSDA+ U study. *Phys. Rev. B* **1998**, *57*, 1505−1509.
(36) Tran, F.; Blaha, P. Accurate band gaps of semiconductors and insulators with a semilocal exchange-correlation potential. *Phys. Rev. Lett.* **2009**, *102*, No. 226401.

https://doi.org/10.1021/acs.jpcc.3c03512
J. Phys. Chem. C 2023, 127, 15630−15640

(37) Kuzmin, A.; Kalinko, A.; Evarestov, R. A. First-principles LCAO study of phonons in $NiWO_4$. *Cent. Eur. J. Phys.* **2011**, *9*, 502−509.
(38) Weitzel, H. Magnetische struktur von $CoWO_4$, $NiWO_4$ und $CuWO_4$. *Solid State Commun.* **1970**, *8*, 2071−2072.
(39) Jiao, Z. J.; Ma, S. H.; Yang, J. F. A comparison of the electronic and optical properties of zinc-blende, rocksalt and wurtzite AlN: A DFT study. *Solid State Sci.* **2011**, *13*, 331−336.
(40) Errandonea, D.; Muñoz, A.; Gonzalez-Platas, J. Comment on "High-pressure x-ray diffraction study of YBO_3/Eu^3+, $GdBO_3$, and $EuBO_3$: Pressure-induced amorphization in $GdBO_3$" [J. Appl. Phys. 115, 043507 (2014)]. *J. Appl. Phys.* **2014**, *115*, 216101.
(41) Birch, F. Finite Elastic Strain of Cubic Crystals. *Phys. Rev.* **1947**, *71*, 809−824.
(42) Anzellini, S.; Burakovsky, L.; Turnbull, R.; Bandiello, E.; Errandonea, D. P−V−T Equation of State of Iridium up to 80 GPa and 3100 K. *Crystals* **2021**, *11*, 452.
(43) Errandonea, D.; Popescu, C.; Achary, S.-N. A. K.; Tyagi, A. K.; Bettinelli, M. In situ high-pressure synchrotron X-ray diffraction study of the structural stability in $NdVO_4$ and $LaVO_4$. *Mater. Res. Bull.* **2014**, *50*, 279−284.
(44) Cliffe, M. J.; Goodwin, A. L. PASCal: a principal axis strain calculatorfor thermal expansion and compressibility determination. *J. Appl. Crystallogr.* **2012**, *45*, 1321−1329.
(45) Tauc, J. Optical properties and electronic structure of amorphous Ge and Si. *Mater. Res. Bull.* **1968**, *3*, 37−46.
(46) Garg, A. B.; Vie, D.; Rodriguez-Hernandez, P.; Muñoz, A.; Segura, A.; Errandonea, D. Accurate Determination of the Bandgap Energy of the Rare-Earth Niobate Series. *J. Phys. Chem. Lett.* **2023**, *14*, 1762−1768.
(47) Rosal, F. J. O.; Gouveia, A. F.; Sczancoski, J. C.; Lemos, P. S.; Longo, E.; Zhang, B.; Cavalcante, L. S. Electronic structure, growth mechanism, and sonophotocatalytic properties of sphere-like self-assembled $NiWO_4$ nanocrystals. *Inorg. Chem. Commun.* **2018**, *98*, 34−40.
(48) Lee, C.; Yang, W.; Parr, R. G. Development of the Colle-Salvetti correlation-energy formula into a functional of the electron density. *Phys. Rev. B* **1988**, *37*, 785−789.
(49) List, N. H.; Kauczor, J.; Saue, T.; Jensen, H. J.; Norman, P. Beyond the electric-dipole approximation: A formulation and implementation of molecular response theory for the description of absorption of electromagnetic field radiation. *J. Chem. Phys.* **2015**, *142*, 244111.
(50) Begum, V.; Gruner, M. E.; Vorwerk, C.; Draxl, C.; Pentcheva, R. Theoretical description of optical and x-ray absorption spectra of MgO including many-body effects. *Phys. Rev. B* **2021**, *103*, No. 195128.
(51) Lima, N. A.; Alencar, L. D.; Siu-Li, M.; Feitosa, C. A.; Mesquita, A.; M'peko, J. C.; Bernardi, M. I. $NiWO_4$ powders prepared via polymeric precursor method for application as ceramic luminescent pigments. *J. Adv. Ceram.* **2020**, *9*, 55−63.
(52) Fujimori, A.; Minami, F. Valence-band photoemission and optical absorption in nickel compounds. *Phys. Rev. B* **1984**, *30*, 957−971.
(53) Burns, R. G. *Mineralogical applications of crystal field theory*, Cambridge Topics in Mineral Physics and Chemistry; Cambridge University Press, 1993, Vol. *5*; pp 1 −551, DOI: 10.1017/CBO9780511524899.
(54) Hush, N. S.; Hobbs, R. J. M. *Absorption Spectra of Crystals Containing Transition Metal Ions*. Prog. Inorg. Chem. 1968, Vol. *10*; pp 259 −486.
(55) Barreda-Argüeso, J. A.; Rodríguez, F. Pressure dependence of the crystal-field spectrum of $KNiF_3$: Single and double excitations. *Phys. Rev. B* **2021**, *103*, No. 085115.
(56) Knox, K.; Shulman, R. G.; Sugano, S. Covalency Effects in $KNiF_3$. II. Optical Studies. *Phys. Rev. B* **1963**, *130*, 512−516.
(57) Ferguson, J.; Guggenheim, H. J. Electronic Absorption Spectrum of Ni (II) in Cubic Perovskite Fluorides. II. Concentration and Exchange Effects. *J. Chem. Phys.* **1966**, *44*, 1095−1102.
(58) Sugano, S.; Tanabe, Y.; Kamimura, H. *Multiplets of Transition-Metal Ions in Crystals*; Acad Press.: New York, 1970; pp 1−348. ISBN: 9780323154796.
(59) Griffith, J.S. *The theory of transition-metal ions* Cambridge University Press, 1964.
(60) Hernandez, I.; Rodriguez, F.; Tressaud, A. Optical Properties of the $(CrF_6)^{3-}$ Complex in A_2BMF_6: Cr^{3+} Elpasolite Crystals: Variation with M− F Bond Distance and Hydrostatic Pressure. *Inorg. Chem.* **2008**, *47*, 10288−10298.
(61) Gavriliuk, A. G.; Trojan, I. A.; Struzhkin, V. V. Insulator-metal transition in highly compressed NiO. *Phys. Rev. Lett.* **2012**, *109*, No. 086402.
(62) Barreda-Argüeso, J. A.; Aguado, F.; González, J. A.; Valiente, R.; Nataf, L.; Sanz-Ortiz, M. N.; Rodríguez, F. Crystal-Field Theory Validity Through Local (and Bulk) Compressibilities in CoF_2 and $KCoF_3$. *J. Phys. Chem. C* **2016**, *120*, 18788−18793.
(63) Karsthof, R.; Anton, A. M.; Kremer, F.; Grundmann, M. Nickel vacancy acceptor in nickel oxide: Doping beyond thermodynamic equilibrium. *Phys. Rev. Mater.* **2020**, *4*, No. 034601.
(64) Bharati, R.; Singh, R. A.; Wanklyn, B. M. Electrical conductivity, thermoelectric power and dielectric constant of $NiWO_4$. *J. Mater. Sci.* **1980**, *15*, 1293−1296.
(65) Gonzalez, J.; Calderon, E.; Capet, F.; Baert, F. Pressure dependence of shallow acceptors in $CuGa(S_xSe_{1-x})_2$ alloys. *Phys. Rev. B* **1998**, *58*, 13654−13659.
(66) Karaouzène, L. I.; Ouahrani, T.; Morales-García, A.; Errandonea, D. Theoretical calculations of the effect of nitrogen substitution on the structural, vibrational, and electronic properties of wolframite-type $ScTaO_4$ at ambient conditions. *Dalton Trans.* **2022**, *51*, 3642−3651.